Springer

Search 🔍 ⚙

Login / Register ▼ | Latin America ▼

Home | Subjects | My Springer | Services | Products | Springer Shop | About us

Monitoring & Environmental Analysis

Home > Environmental Sciences > Monitoring & Environmental Analysis

SUBDISCIPLINES | JOURNALS | BOOKS | SERIES | TEXTBOOKS ✉ ➕

Environmental Monitoring and Assessment

An International Journal Devoted to Progress in the Use of Monitoring Data in Assessing Environmental Risks to Man and the Environment

Editor-in-Chief: G. B. Wiersma

ISSN: 0167-6369 (print version)
ISSN: 1573-2959 (electronic version)

Journal no. 10661

Read Online

▶ ☰ | 🔒 RECOMMEND TO LIBRARIAN

g+1 4

ABOUT THIS JOURNAL | EDITORIAL BOARD | ETHICS & DISCLOSURES

READ THIS JOURNAL ON SPRINGERLINK

All volumes & issues ⟴

Free: Sample Articles ⟴

FOR AUTHORS AND EDITORS

2013 Impact Factor | 1.679

Aims and Scope ⟴

Submit Online ⟶

Open Choice - Your Way to Open Access ⟴

Instructions for Authors ⟴

Instructions for Authors Part II ⟴

SERVICES FOR THE JOURNAL

---

g+1 4

Instructions for Authors Part II ⟴

ABOUT THIS JOURNAL | EDITORIAL BOARD | ETHICS & DISCLOSURES

SERVICES FOR THE JOURNAL

Contacts ⟴

Download Product Flyer ⟴

Shipping dates ⟴

Order back issues ⟶

Bulk Orders ⟴

Article Reprints ⟴

ALERTS FOR THIS JOURNAL

Get the table of contents of every new issue published in Environmental Monitoring and Assessment.

Your E-Mail Address

SUBMIT

☐ Please send me information on new Springer publications in Monitoring / Environmental Analysis.

RELATED BOOKS - SERIES - JOURNALS

Book

Vehicular Air Pollution and Urban Sustainability

Author» Thornbush, Mary J.

Your article in Environmental Monitoring and Assessment (4676): Information Required
Springer [springerauthorquery@springeronline.com]

Enviado el: miércoles, 10 de junio de 2015 04:32 a.m.
Para: RODRIGUEZ MORENO VICTOR MANUEL

Springer

Springer: My Publication   10.06.2015

visit us at springer.com

Important Announcement

Dear Author,

Thank you for publishing with Springer. This message is to let you know that your article

- Article title: The geospatial relationship of geologic strata, geological fractures, and land use attained by a time-series aridity index in a semiarid region
- DOI: 10.1007/s10661-015-4676-2

has gone into production. Before we can send you your proofs, we have to ask you to provide some additional information. Please go to the following website (you may need to copy and paste the URL into your browser): http://www.springer.com/home?SGWID=0-0-1003-0-0&aqId=2866206&checkval=93e5b28b6cb0987272da3f1f04413280

Please indicate if you would like to:

2

The geospatial relationship of geologic strata, geological fractures, and land use attained by a time-series aridity index in a semiarid region

Victor M. Rodríguez-Moreno[a], Thomas G. Kretzschmar[b] and J. Saúl Padilla-Ramírez[a]

[a] Instituto Nacional de Investigaciones Forestales, Agrícolas y Pecuarias (INIFAP). Experimental Field Station Pabellón, km 32.5, highway Ags-Zac, ZP 20660, Pabellón de Arteaga, Aguascalientes, México. Tel/Fax +52 465 9580161.

[b] Centro de Investigación Científica y de Educación Superior de Ensenada (CICESE), Department of Geology, highway Ensenada-Tijuana No. 3918, ZP 22860, Ensenada, Baja California, México.

[a] Corresponding author: rodriguez.victor@inifap.gob.mx

ABSTRACT

In a vast semiarid region of the Baja California Peninsula remote sensing and GIS techniques were applied to moderate resolution images of Landsat 5 TM to explore the geospatial correlation among the grid aridity index (AI), shapefiles of geologic strata, land use, and geological fractures. A dataset of randomized sample points in a time series of one hydrologic year along with vector files GIS delineated geologic fractures--including the area between their left/right parallel buffer lines, were used as mask analysis. MANOVA results were significant ($p<0.05$) for geologic strata, land use, and basin. Overall results reveal the effects of soil texture on water retention on deeper soil horizons and the rate of vertical motion of rainwater. Despite the fact that geologic fractures underlie a large number of biotic communities, in both latitude and longitude gradients of the peninsula, no statistical significance was observed among the fractures themselves or the areas between their parallel buffer lines. One pulse rainfall event was documented by the AI grid maps enabling a robust vegetative response in early summer to an abnormal amount of rain provided by tropical storm Julio. AI grids appear to be useful for characterizing an ecosystem's dynamism. New options are suggested for this research strategy by expanding the number of datasets and incorporating geographic exclusion areas.

Keywords; aridity index, geospatial analyses, geologic fractures, semiarid ecosystem

INTRODUCTION

Desert and semiarid landscapes are subject to extremely irregular rainfall regimes, characterized by their meagerness and infrequency. This fact, along with the properties of geological strata for holding water, explains why vegetation grows in patches and why plants evolve physiological mechanisms for preserving it. These mechanisms

include the reduction of gas exchange by the opening/closing of stomates, water storage for future short-term requirements, and modification of the exposure angle to the sun for keeping internal temperature low, along with protecting the photosynthetic system.

Matin and Goswami (2012) mention that dryland ecosystems regulate their own micro-climates. Their vegetation cover determines the surface reflectance of solar radiation as well as water evaporation rates. In arid and semiarid regions soil moisture, when available throughout the year, is often the only water resource (Wang 2008). The timing and management of this resource is absolutely essential for understanding plant spatial distribution and for identifying recharge areas which are apparent in vegetative greenness and aridity indices. According to Wang (2008), groundwater basins can be viewed as nested systems of recharge and discharge, with discharge apparent in the form of springs, streams, and evapotranspiration. In arid environments, the understanding of land–atmosphere exchanges is complicated by the episodic nature of precipitation, extremely dry soil moisture, considerably small recharge potential (i.e., the difference between precipitation and evapotranspiration), and vegetative controls, along with spatial complexity and scaling (e.g., Scanlon et al. 2002; 2003; 2005; Walvoord et al. 2002; Newman et al. 2006). Maxwell (2010) suggests that subsurface heterogeneity, particularly in fractured systems, further complicates the distribution and movement of subsurface moisture. This subsequently affects the spatial and temporal distribution of land–atmosphere exchanges.

Identifying groundwater recharge and discharge areas across catchments is critical for implementing strategies for surface and groundwater resource management and ecosystem protection (Tweed, et al. 2006). Physical and mineralogical properties of strata strongly influence the configuration of functional vegetation types through water retention and soil resources. This relationship with water and soil formation can be better understood by studying the geological properties of the media, the manner of their formation, and their interaction with climate factors. Jackson et al. (2004) reference a number of investigators who have explored the potential of using reflectance data to estimate Vegetation Water Content (VWC); they mention that the Normalized Difference Water Index (NDWI) (Gao 1996) and the Normalized Difference Infrared Index (NDII) (Hardinsky 1983) are related to VWC. Both indices share the same general equation form, based on contrasting reflectance on NIR and SWIR through its normalization. Subsequently, Abbott and Refsgaard (1996) mention that hydrological models can fulfill the need of describing spatial heterogeneity, assessing the impact of naturally and humanly induced changes, and providing detailed descriptions of the hydrological processes in watersheds for satisfying various needs in spatial modeling. These models, however, require spatially acquired data as input for reflecting the heterogeneity of base information in watersheds. Spatial rainfall is one of the key inputs for these models and, likewise, the accuracy of

4

stream flow predictions from a hydrological model is greatly dependent on the accuracy of rainfall inputs (Gourley and Vieux 2006). Therefore, the accurate estimate of rainfall patterns over a catchment and a region is a great concern (Kurtzman et al. 2009), along with other meteorological variables, such as temperature, relative humidity, insolation, and evaporation rate.

Since establishing and maintaining a network of gauges in large scale ecosystems demands resources in technology, time, and money, remotely sensed images represent a confident and cheaper way to collect data in the absence of weather stations. Currently, it is both economically and practically impossible to significantly increase the number of rain gauges for registering spatial rainfall (Taesombat and Sriwongsitanon 2009). As an alternative, the use of satellite-based and radar-based weather datasets (He et al., 2011) drive in rainfall estimates for hydrological modeling. These datasets has the potential to improve our capability for reducing uncertainty in rainfall inputs (Sawunyama and Hughes 2008).

Vegetation studies using remotely sensed images have generally been used to determine rock type relating to problems of interpreting reflectance from open shrub lands (Rodriguez-Moreno and Bullock, 2015). However, rock type delineates landscape units that may differ in vegetation structure and function (Franco-Vizcaino et al. 1993; Bedford et al. 2009). There are disparate mechanisms for such effects, some related to soil texture or chemistry (Graham and Franco-Vizcaíno 1992; Jenny 1941), and others to the fracturing and weathering of rocks which affect water storage (Tuğrul 2004). In semiarid and arid regions, slopes and weathering are not always conducive to the development of broadly representative soil profiles, and rock type may be a useful key for determining their properties. According to Liang et al. (2011), satellite-reflectance based aridity and drought indices are important for clarifying the effect of environmental parameters relevant to temporal characteristics of land surface temperature, the surface energy balance model, assuming that land surface temperature, solar flux, and air-temperature sinusoidal change are considered.

The present study integrates regular temporal satellite images of the aridity index (AI) covering almost one hydrological year for indirectly investigating the spatial distribution of water availability in a semiarid ecosystem. This ecosystem is characterized by a high number of fractured systems, a set of interrelated processes of water and energy exchanges from the land surface, a variety of geological strata, and land use. To provide a more realistic and less complex picture of surface properties, a multi-temporal grid dataset of AI was grouped with a multiple and fully integrated model for mapping its spatial variability. Through the analysis model, we evaluate the effect of various time-stable geomorphic attributes in the environment relevant to the soil-water availability-vegetation relationship. The region studied is characterized by complex topography, geology, and climatology--also

by a wide variety of plant adaptations, especially by perennial plants, to low water availability (Rodríguez-Moreno and Bullock 2013). Two central questions were addressed in this study: 1) What are the influences of subsurface heterogeneity on spatial patterns in the aridity index?; 2) What is the relationship between AI surface expression and the underlying infiltration rates and subsurface moisture in the semiarid ecosystem?

MATERIALS AND METHODS

Description of the study area

The study area is dominated by desert and shrub ecotypes, except in the coastal areas where plant communities are dominated by coastal scrub, also called soft chaparral. The central region of the Baja California Peninsula is an exceptional area for the study of hydro-geological issues. This region has a dry, tropical desert climate characterized by a mean annual precipitation less than 100 mm. In addition to its lengthy extension (1,100 km in latitude; 22.87° to 31.81°N), ecosystems grow under the influence of a highly variant climate, from intra-tropical to low temperate latitudes. They are also affected along North-South and East-West gradients by temperate, tropical, regional, and local circulations (Dettinger 2004; Douglas et al. 1993; Reyes and Mejía-Trejo 1991). The East-West gradient is bracketed by the warm waters of the Gulf of California, low plains and adiabatically dried air, contrasting with the cool waters and moist, cool ocean breezes of the Pacific. Mountain terrain extending along the peninsula divides the hydrological regions into western and eastern basins. Most of the aquifers are composed of fluvial and marine sediments in coastal quaternary alluvial fans and coastal plains. The geological structure is much more complex and rougher than the North American basin and range province (Gastil et al. 1975); there is wide representation of extrusive and intrusive igneous, metamorphic, and sedimentary rock types. Overall, the geology of Baja California is composed of intrusive Cretaceous rocks belonging to the peninsular batholith, extrusive rocks of Tertiary and Cretaceous ages, along with Mesozoic metamorphic material (Daesslé at al. 2008). A geological summary made by Cotton and Western Mining, Inc. (2008) mentions that the batholith is cut by a number of faults oriented mostly towards a northwest to northeast direction. These are probably related to mountain forming movements in the Cretaceous to Tertiary periods. Acidic extrusive rocks are shown in the area covering the older intrusive rocks. Rocks observed in the field are mostly andesite mixed rhyolite. Sedimentary rocks range in age from the Jurassic to early Cretaceous periods. They have all been intruded by the batholith and other smaller intrusive bodies. Contact metamorphic rocks including some marble have formed adjacent to the igneous intrusive. Cretaceous sediments are of the post batholith age and consist of sandstone and conglomerates, mostly derived from volcanic rocks. Quaternary gravels and alluvium cover the valleys and low areas between the mountains.

Limits of the study were defined by the continental land in Landsat 5 TM images designated path 37, row 40. A random function was applied on the image spatial boundary; along with randomness, the location of points was restricted by an additional criterion, a 200 m buffer between each. A sample dataset of 3,900 pixel centroid coordinate pairs of Landsat 5 TM pixels (~900 sqm each) (Fig. 2) was obtained. This dataset was used as point extracting mask from serial grids of the AI, elevation, clay, sand, and loam. A digital elevation model (DEM) of one arc per second resolution (~30 m), provided by the Instituto Nacional de Estadística y Geografía (INEGI) of Mexico, was adjusted by filling gaps and sinks. Because the study area is characterized by complex geomorphology, to calculate the basin area and its spatial limits we had to resolve a depression issue, where the summation of upslope area stopped, by filling the depressions up to the lowest elevation in the neighboring cell. This resulted in flat areas where most of the flow routing algorithm also stopped. Following the procedure recommended by SAGA-GIS v 2.1.0 developers, to provide valid catchment area calculation, we select the DEM as input and preserve a minimal slope in the filled areas by specifying a 0.01 degree slope. The channel network was traced through DEM data and Flow Direction, with a minimum segment length of 10 m. Spatial limits of basins, the sink route, and channel network were delineated through the DEM by applying the Kinematic Routing Algorithm (SAGA-GIS 2013). Fractures in rock type were digitized from scanned geologic cards (1:250,000 scale); buffer lines parallel to the left and right of each fracture were delineated 100 m apart (Fig. 1). A land use map is available from previous studies based on field and satellite data from INEGI (Fig. 2). Plant communities were defined by their ecological, floristic, physiognomic, and phenological characteristics, as well as by their degree of conservation/degradation.
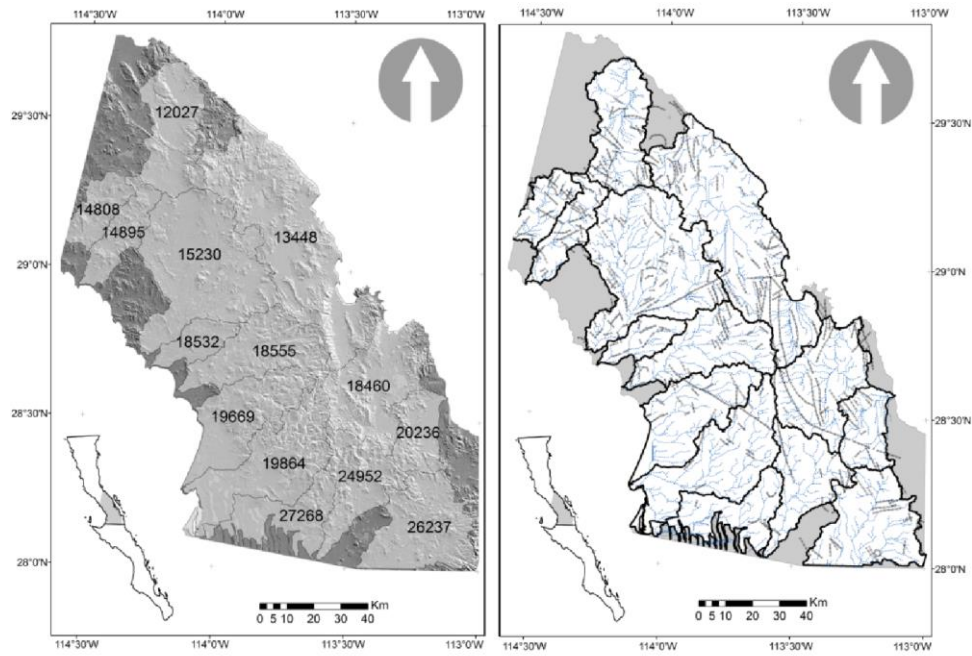
Figure 1. Major catchment spatial limits and assigned codes (left). Geological fractures and channel network (right).
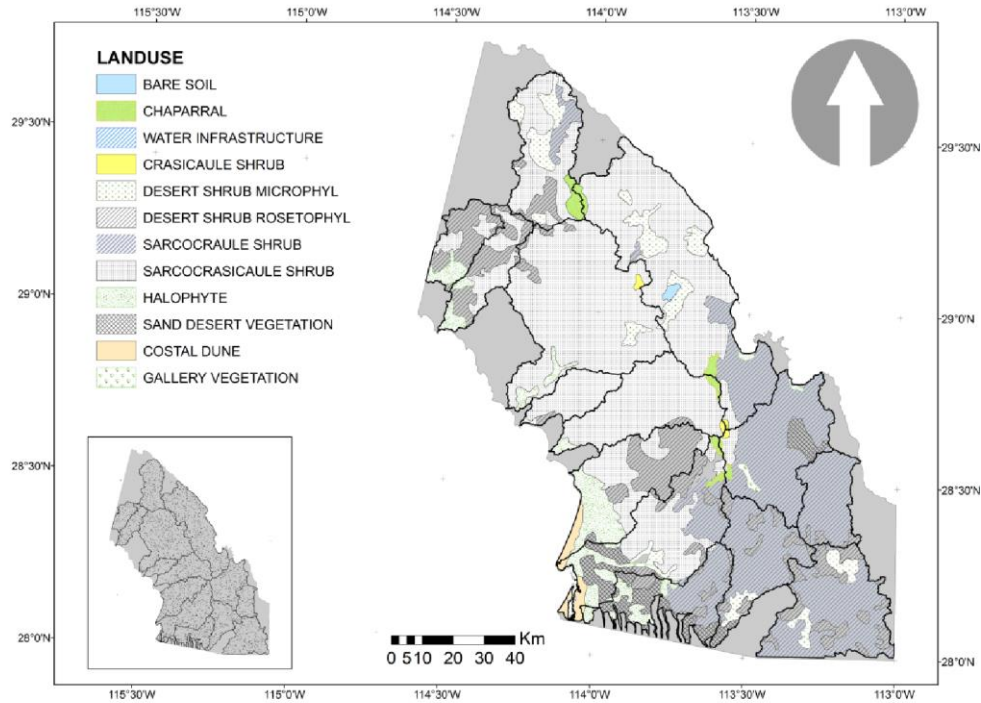
Figure 2 Land use of the study area; spatial limits were based on a scale of 1:250 000. In the inner square, 3,900 randomized sample points are located

Table 1. Regional descriptive statistics by catchment based on the sample dataset

CODE	AREA (sqkm)	*n*	ELEV (masl)	CLAY (%)	SAND (%)	LOAM (%)	CIC (meq/100 g)	EC (ds/m)	Mg	OM	pH
12027	921	262	484	17.7	61.5	21.9	13.5	1.7	3.8	0.8	8.0
14808	390	100	438	11.7	70.6	18.4	9.4	1.2	2.9	0.7	7.6
14895	473	156	424	24.0	48.6	26.1	18.1	4.0	7.5	1.0	8.0
15230	2009	553	387	20.8	54.2	23.6	15.4	3.2	6.6	0.9	8.0
18532	319	70	422	11.9	69.4	18.3	9.2	1.2	3.8	0.7	7.4
13448	2325	685	367	13.4	68.6	17.8	12.5	1.1	2.9	0.5	7.4
18555	938	260	213	17.1	58.6	24.0	11.5	1.4	3.7	1.0	7.6
18460	1064	321	539	17.9	61.3	20.8	13.6	1.5	3.8	0.9	7.6
20236	484	132	394	22.3	59.7	18.0	16.8	2.5	4.8	0.8	7.7
19669	986	291	437	19.0	66.0	15.1	15.0	2.5	4.2	0.8	7.6
19864	1283	345	363	12.8	70.2	16.8	12.5	1.1	2.9	0.4	7.4
27268	673	205	640	17.7	62.9	18.7	15.2	1.4	4.0	0.7	7.4
24952	762	207	536	15.5	66.3	18.3	14.7	2.3	4.2	0.7	7.2
26237	1095	313	273	15.5	68.4	16.0	12.4	2.0	3.3	0.8	7.6

From Table 1, the CODE column refers to catchment; AREA is estimated based on the number of pixels within the catchment's spatial limits; *n* stands for the number of pixels within the spatial limits of the catchment and each represents ~900 m^2 (~0.0009 km^2) in the terrain; the simple ratio between catchment area and sample size range from 0.02 % to 0.03 %; the ELEV column is for Elevation data; the clay, sand, and loam columns indicate soil texture; CIC is for Cationic Interchange Capacity; EC is for Electric Conductivity; Mg is for magnesium content; OM, is for organic matter; and pH is the acronym for "*pondus Hydrogenium*" which indicates substance acidity.

Regional soil texture (i.e. the amount of clay, sand, and loam) in the study area is definitely characterized by a high percentage of sand (range, 48.6-70.6), followed by loam (range, 15.1-24.0), and clay (range, 11.7-24.0). The EC, a property referring to the amount of soluble salt in soil, represents the ability of an aqueous solution to carry an electric current; it has been reported to affect plant growth (physically and chemically), and this is especially important in arid and semi-arid lands. Data indicated that the highest mean values of EC matched the highest clay content in catchments 14895 and 15230. This relationship was also very close for CIC, where the same catchments had the highest mean values (18.1 meq/100g and 15.4 meq/100g) respectively. In arid and poorly drained soils the rate of evaporation is usually higher than the rate of infiltration, and this phenomenon is associated with an accumulation of salt near the soil surface. This was observed in particular for pH; the regional pH trend is alkaline.

Data Preparation and Analysis

Landsat 5 TM satellite images were reviewed for relative radiometric, atmospheric, and topographic (illumination) corrections. Multi-temporal variability was evident in 14 images. Substantially cloud-free images were selected and these covered a period from summer of 2008 to spring of 2009. Specific dates for the images were: July 6, August 7, September 8, October 10, October 26, November 11, and December 29 of 2008; January 14, January 30, March 3, March 19, April 4, April 20, and May 6 of 2009.

One vegetation index, based on contrasting red and infrared light, is the Normalized Difference Vegetation Index (NDVI) (Eq. 1); another, the aridity index (AI), is based on the standardized NDVI (Eq. 2). Both indices were calculated for the entire period; they employed the complex and fully integrated model for mapping the spatial variability of land use. The AI is widely used for climate-based land classification from a dryness perspective (Arora, 2002), and is used here for two reasons: 1) to obtain a rate-of-change estimate using the time-series analyses; and 2) to explore, using its 3D profile, the AI-geological fracture's relationship to identify potential geographic zones for ground water recharge.

$$NDVI = \frac{(RED - NIR)}{(RED + NIR)} \tag{1}$$

$$AI = \sqrt{\frac{1}{n}\sum_{i=1}^{n}(NDVI_i - NDVI_{mean})^2} \tag{2}$$

All elements of Eq. 1 are based on reflectance data at ground level: RED stands for reflectance in the red band (0.63 – 0.69 μm) and NIR for reflectance in the near infrared band (0.76 – 0.90 μm). The range of values for NDVI is -1 to +1. In Eq. 2, *n* indicates the number of scenes (images) included in the study, $NDVI_i$ is the index value on each image date; $NDVI_{mean}$ is the NDVI mean value for the entire period. The range of values for AI is greater than zero and less than one (0<AI<1). While the NDVI has proven useful for a timely estimation of vegetation condition, as a normalized ratio it does not provide for relative comparison at a pixel location or for a time period (Burgan and Hartford 1993; Kogan 1990; Kogan 1995). The ability to compare pixel values in this way is useful for removing seasonal vegetation changes and for facilitating an interpretation of different vegetation cover using the historical record. According to Peters, et al. (2002), this per-pixel data expressed as Standardized NDVI, is an estimate of "probability of occurrence" of the present vegetation condition; zero is the baseline condition in which a pixel NDVI value is lower than all possible NDVI values in other scenes.

Subsequently, when taking into account that one hydrologic cycle is under study, AI values for mapping purposes and data interpretation were grouped into five classes, each one comprising different and consecutive value ranges. These classes are termed very arid (0<AI<0.05), low arid (0.05 <AI<0.25), average arid (0.25<AI<0.75), not

arid (0.75<AI<0.95), and comfortable (0.95<AI<1). This class distribution is intended to mimic a normal-probability density function, so the mean of AI for the location and time period is zero. The very arid class occurs when pixel continuously reaches 0.05 or less and ends when the AI becomes greater than 0.05. For example, classifying a pixel as "very arid" indicates that its NDVl value is lower than average in one scene of the cycle relative to that in other scenes of the study. A pixel classified as "comfortable" is an indication that its value is higher than average or that the vegetation is in good condition. Because the AI is obtained from NDVI, the NDVI data is omitted from statistical analyses.

Class names for land use, as represented in the legend of Fig 2, will be handled and reported hereafter in abbreviated form as: Bare soil (BARE), Chaparral (SHRUB), Water Infrastructure (WI), Crasicaule shrub (CRASIC), Desert Shrub Mycrophyl (DSM), Desert Shrub Rosetophyl (DSR), Sarcocraule Shrub (SS), Sarcocrasicaule Shrub (SSc), Halophyte (VH), Sand Desert Vegetation (SDV), Coastal Dune (CD), and Gallery Vegetation (GV).

The randomly distributed sample dataset based on the spatial limits of basins (Fig. 2, inner square) was used for testing the assumption of normality in the AI data, and it was analyzed based on the Shapiro and Wilk's test (Royston, 1995) where the α level =0.05. Regional analysis was performed at basin scale. Along with the normality test, the Multivariate Analysis of Variance (MANOVA) and the post-hoc Bonferroni test were performed. The first reason for using MANOVA instead of ANOVA for analyzing data is that it is able to take into account multiple independent and multiple dependent variables within the same model, thus permitting greater complexity. Secondly, rather than using the F value as indicator of significance the Wilk's lambda test is used; this demonstrates the amount of variance revealed in dependent variables by independent variables; the smaller the value, the larger the difference between the groups being analyzed. (One) 1 minus Wilks' lambda indicates the amount of variance in the dependent variables revealed by the independent variables. The multiple comparison methods examine or compare more than one pair of means or proportions at the same time. The post-hoc Bonferroni test is a multiple comparison test widely used in statistical analysis of equal and unequal sample sizes. It assumes that the user wants to test all possible pairs of linear combinations or comparisons of treatment level means. As cited by NIST/SEMATECH (2015), when comparing it with other multiple comparison methods, Bonferroni is adequate when the number of contrasts to be estimated is small, (about as many as there are factors); actually, unless the number of desired contrasts is at least twice the number of factors, Scheffé will always show wider confidence bands than Bonferroni.

RESULTS

The regional model analysis included the AI time-series data for all dates as a dependent variable and the categorical factors for basin, land use, and geological strata as independent variables. All factor codes were incorporated in the analysis and the intervening effects were eliminated. Three of the land use categories (GV WI, and CD) were not considered because of the low number of sample points in order to prevent a bias when interpreting results. MANOVA model results suggest that time-series variation in AI was influenced mostly by the geological strata (Wilk's=0.68, F [56, 14,966] = 27.49, p<0.01), and less by land use (Wilk's=0.82, F [140, 31,586] = 5.31, p<0.01) and basin (Wilk's=0.86, F [182, 36,924] = 3.25, p<0.01).

Geological Analysis

In Fig. 3 the serial pattern of AI by image date reveals that all geologic strata reached their maximum mean value on September 8th, except SND_CGMD where it occurred on December 29th. These results, considering the proposed classes for AI, suggest that in September the association of land use with regional geology study was observed in the average arid category (>0.25 AI<0.75). This regional condition was observed in August, December, and January; remarkably the largest separation among geologic strata occurred in September. A low arid condition (>0.05AI<0.25), however, was observed in July, October, November, and from March to May.
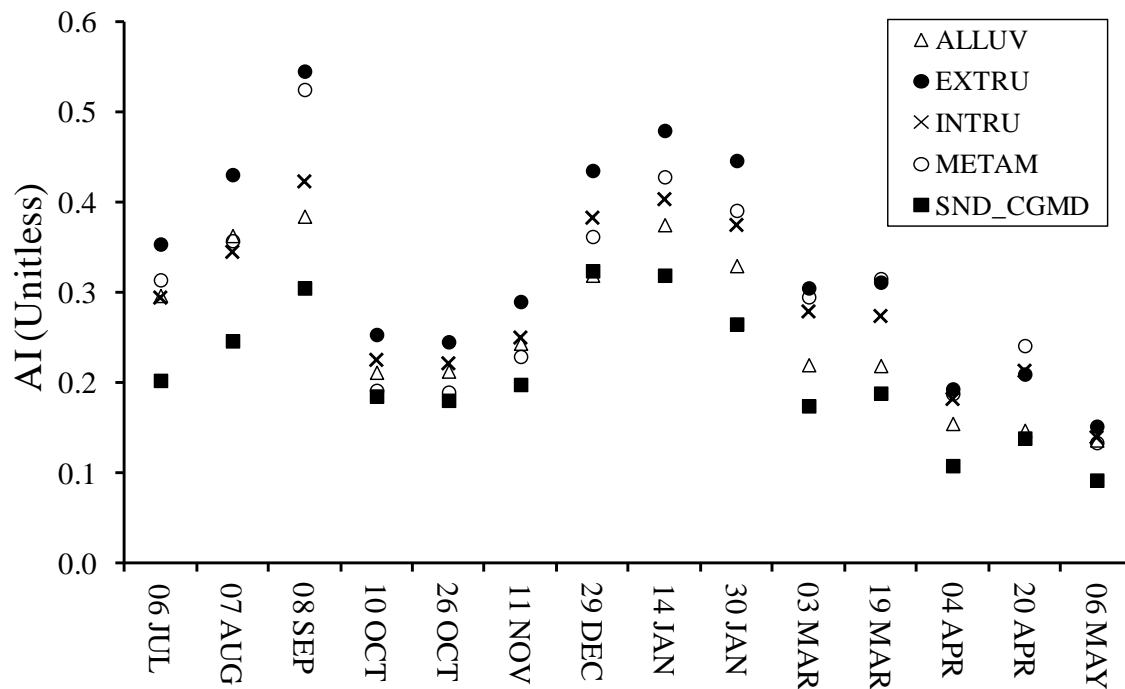
Figure 3. Temporal series of the AI dataset by geologic strata. The means represent the entire sample dataset.

In Fig. 3, apart from the geologic strata, an abnormal increase in AI is observed in September and seems to indicate that a rainfall pulse occurred; evidence for this is provided by the abrupt decrease in AI on the following date (October). Furthermore, except for the September date, a bimodal distribution pattern for AI is observed which is

12

concurrent with the two periods of seasonal rainfall, one during winter and the other from late spring to early summer. Maximun AI values observed for September and mid-January seem concurrent with tropical storm Julio in late August and the rainy winter season, respectively. These results support those reported by Balba (1995) that in a sandy stratum rain penetrates deeper than in fine-textured soils but holds less water for plant uptake. In addition, less water is subject to loss by evaporation, and therefore in areas with low rainfall and soils with sandier texture, a high infiltration rate can be considered beneficial. This benefit is mainly on promoting an increase of groundwater. Plant communities may suffer periods of commonly frequent drought due to water scarcity and poor soil fertility. In contrast, the mineralogical properties and fine texture of the METAM and EXTRU substrates react in an opposite manner; these substrates tend to preserve water in upper soil horizons, favoring enhancement of the root zone, but resulting in increased evaporation rate, except during heavy rains where it promotes the horizontal motion of water. Their permeability properties to allow water to pass through it tend to preserve water in deeper soil horizons when available. This was observed in September, days after tropical storm Julio, and in the early winter of January (Table 2).

Table 2. The AI regional time-series of rock types. The highlighted data are the maximum AI value among the strata on each date, and the underlined, the minimum. The lower letter is the Bonferroni test for homogeneous groups (α=0.05)

DATE	GEOLOGIC STRATA				
	SND_CGMD	INTRU	ALLUV	METAM	EXTRU
06 JUL	0.202	0.293	0.295	0.313	**0.354**
	b	a	a	a	c
07 AUG	0.246	0.344	0.363	0.357	**0.431**
	b	a	a	a	c
08 SEP	0.304	0.422	0.384	0.524	**0.545**
	b	d	c	a	a
10 OCT	0.185	0.224	0.211	0.191	**0.253**
	a	c	bc	ab	d
26 OCT	0.180	0.220	0.212	0.189	**0.245**
	a	c	bc	ab	d
11 NOV	0.198	0.249	0.243	0.228	**0.290**
	b	a	a	a	c

29 DEC	0.323	0.382	0.318	0.361	**0.435**
	a	b	a	b	c
14 JAN	0.319	0.402	0.374	0.427	**0.480**
	b	a	c	a	d
30 JAN	0.264	0.373	0.329	0.390	**0.446**
	b	a	c	a	d
03 MAR	0.174	0.278	0.219	0.294	**0.305**
	c	a	d	ab	b
19 MAR	0.187	0.273	0.218	**0.314**	0.311
	b	d	c	a	a
04 APR	0.107	0.181	0.154	0.187	**0.193**
	c	a	d	ab	b
20 APR	0.138	0.212	0.146	**0.240**	0.209
	a	b	a	c	b
06 MAY	0.091	0.138	0.136	0.133	**0.151**
	b	a	a	a	c

In Table 2, we notice that the AI minimum and maximum mean values ranged from the low arid class to the average arid class. In view of the expression of AI as an indicator of the spatial dynamism of ecosystems in time-series data, results indicate significant differences ($p<0.05$) among strata. It is remarkable that we observed two extremes in soil water holding capacity. On one hand, poor water retention was observed for the SND_CGMD stratum with regional minimum mean on almost all dates, except in early winter (December), while the EXTRU stratum showed the highest AI mean data on all dates with water available for plant uptake. These results seem to indicate that serial AI matched well with rain seasonality because of its timing response to humid conditions. For example, from September 8th to October 10th, a noticeable decrease was observed in AI (-0.119); from November 11th to December 29th a positive increase was noted (+0.125), which matches well with the start of the winter rainy season. Coinciding with the peak of the winter rainfall season, in mid-January the AI reached its maximum value and from there to the last date of the study (May 6th) a progressive decrease was observed, until the AI reached its minimum (0.091). On September 8th all strata registered their maximum AI values, except for SND_CGMD. This fact seems to validate the observation that a rain pulse occurred on this date, since we had observed the lowest aridity

14

value in the entire period. Much of the pulse-reserve theory has been developed using the response of desert plants to precipitation as a system model (Anderson et al. 2008; Chesson et al. 2004; Noy-Meir 1973; Schwinning and Sala 2004). This study, therefore, provides ample proof for the assumptions mentioned above using satellite AI index. On May 6th time-series data were all observed in the "low arid" class, the lowest AI values of all geologic substrates observed in all time-series data.

Since clay soils hold water more tightly than loam and sandy soils, soil surface and water absorption features will be more prominent in clayey soils, given the same amount of time since the last precipitation or watering. Our study demonstrated that the ALLUV and SND_CMG strata are spatially located on flat areas. The geological stratum ALLUV is formed mainly by the deposition of minerals made by flood waters and subjection to sedimentation forces. The SND_CMGD, however, is a granular stratum consisting of rocks and mineral particles that are very small; the soil texture is therefore gritty and sandy, and is formed by the disintegration and weathering of rocks such limestone, granite, quartz, and shale. Pertinent to permeability and water retention, some components of ALLUV can absorb more than their weight in water, while other components are responsible for over-drainage and the dehydration of soil-cover plants during the summer season; it warms up quickly in spring. As observed following September 08th, which seems to resemble a rain pulse event, the increment of change from September to October ranged from 6% for ALLUV to 47% for METAM. This change was followed by a decrease immediately after the next data date (October 10th) which ranged from -39% for ALLUV to -64% for METAM. This increment/decrement rate from one date to the next was not observed in the rest of the date data, and seems to support the occurrence of a rain pulse event. A possible explanation for this observation may be delivered by Rodríguez-Moreno and Bullock (2015) in another study of the same region; they provided linear models to prove the influence, as of September 8th, of a period of accumulated rain on vegetative expression 4 to 6 weeks before the image date acquisition.

Land Use

Regional analysis by land use includes only 11 of the 12 classes because of the exclusion of WI due to its insignificant data in the database (12 pixels). The results are shown in Table 3.

Table 3. Regional land use analysis of AI by class. Bold data indicates maximum AI; underlined data indicates the minimum.

LAND USE	06 JUL	07 AUG	08 SEP	10 OCT	26 OCT	11 NOV	29 DEC	14 JAN	30 JAN	03 MAR	19 MAR	04 APR	20 APR	06 MAY
BARE	0.27	0.38	**0.43**	0.19	0.19	0.22	0.26	0.34	0.27	0.18	0.24	0.14	<u>0.11</u>	0.11

CD	0.25	0.32	**0.38**	0.17	0.18	0.20	0.30	0.36	0.32	0.21	0.20	0.14	<u>0.12</u>	0.12
CRASIC	0.22	**0.54**	0.16	0.21	0.21	0.24	0.25	0.34	0.33	0.19	0.15	0.14	<u>0.11</u>	0.18
DSM	0.35	0.41	**0.52**	0.23	0.23	0.28	0.38	0.46	0.41	0.27	0.28	0.20	0.18	<u>0.16</u>
DSR	0.32	0.37	**0.50**	0.21	0.21	0.25	0.38	0.42	0.39	0.26	0.28	0.17	0.19	<u>0.14</u>
SDV	0.31	0.38	**0.44**	0.21	0.21	0.25	0.34	0.41	0.37	0.24	0.24	0.17	<u>0.13</u>	0.14
SHRUB	0.32	0.39	**0.46**	0.26	0.25	0.28	0.41	0.45	0.41	0.28	0.30	0.18	0.21	<u>0.16</u>
SS	0.36	0.45	**0.49**	0.27	0.27	0.30	0.46	0.48	0.44	0.32	0.33	0.20	0.25	<u>0.16</u>
SSc	0.23	0.27	**0.35**	0.18	0.18	0.20	0.31	0.33	0.29	0.20	0.20	0.13	0.15	<u>0.10</u>
GV	0.30	0.34	**0.38**	0.21	0.20	0.24	0.31	0.34	0.31	0.23	0.20	0.16	<u>0.12</u>	0.13
VH	0.33	0.39	**0.54**	0.22	0.23	0.28	0.37	0.46	0.41	0.27	0.29	0.20	0.18	<u>0.15</u>

From Table 3 our data seem to document the fact of a rain pulse because all land-use classes, except CRASIC, reached their maximum AI value in September and their minimum in late spring. It is clear that tropical storm Julio, which affected the peninsula in late August, definitely influenced vegetative expression; hence we observe a possible pulse and resource variability here. Among land use classes, SS was consistent in maintaining the maximum AI value after September 8th. Minimum AI values were maintained by three classes: CRASIC, SSc, and BARE. In general terms, our results readily demonstrated that vegetation communities responded to humid conditions as observed on September 8th when the maximum AI value was recorded; it was not surprising that the BARE class had not registered the minimum AI value in all time-series data. We had to deduce a possible mask effect of soil moisture on decreasing the reflectance rate, thereby influencing the AI value. On arid and semiarid surfaces some soils or rocks are covered by biogenic crusts of different microphytic communities, comprised of mosses, lichens, liverworts, algae, fungi, cyanobacteria (used called blue-green algae), and bacteria (West 1990). Our results seem to confirm what Karnielli, et al. (1999) documented about the role of biogenic crusts; when wet, their NDVI value can reach 0.30 units due to their photosynthetic activity. This may be the reason why in September BARE and CD, the two classes that are composed of rocks and sand, had reached a maximum AI value comparable to other classes where vegetation is present.

Basin Analysis

Table 4. Regional analysis of AI by basin. Bold data indicate the maximum mean value; the underlined indicate the minimum.

BASIN	06 JUL	07 AUG	08 SEP	10 OCT	26 OCT	11 NOV	29 DEC	14 JAN	30 JAN	03 MAR	19 MAR	04 APR	20 APR	06 MAY
12027	0.361	0.392	**0.523**	0.217	0.227	0.268	0.351	0.469	0.430	0.315	0.307	0.213	0.198	**<u>0.171</u>**
13448	0.338	0.402	**0.556**	0.231	0.227	0.295	0.388	0.452	0.417	0.279	0.287	0.209	0.211	**0.160**
14808	0.360	0.453	**0.491**	**<u>0.095</u>**	0.102	0.131	0.182	0.302	0.377	0.280	0.243	0.191	0.199	0.145
14895	0.298	0.363	**0.465**	**<u>0.097</u>**	0.101	0.136	0.194	0.253	0.271	0.340	0.216	0.165	0.178	0.133
15230	0.174	0.201	**0.306**	0.106	0.113	0.125	0.224	0.248	0.213	0.144	0.157	0.087	0.135	**<u>0.071</u>**
18460	0.292	**0.495**	0.490	0.289	0.282	0.312	0.378	0.419	0.377	0.232	0.286	0.175	0.174	**<u>0.134</u>**
18532	0.185	0.212	0.215	0.147	0.144	0.143	0.258	**0.273**	0.229	0.128	0.116	0.085	0.120	**<u>0.070</u>**
18555	0.258	0.304	**0.458**	0.140	0.138	0.166	0.244	0.340	0.325	0.298	0.300	0.162	0.208	**<u>0.106</u>**
19669	0.341	0.424	0.423	0.160	0.156	0.193	0.370	**0.488**	0.441	0.300	0.280	0.164	0.145	**<u>0.126</u>**
19864	0.430	0.469	0.467	0.295	0.289	0.316	0.539	**0.567**	0.510	0.358	0.336	0.232	0.231	**<u>0.195</u>**
20236	0.246	0.245	**0.420**	0.288	0.269	0.279	0.412	0.350	0.296	0.169	0.205	0.108	0.192	**<u>0.101</u>**
24952	0.368	0.382	0.375	0.393	0.367	0.397	**0.643**	0.559	0.492	0.314	0.339	0.209	0.247	**<u>0.169</u>**
26237	0.181	0.227	0.317	0.303	0.294	0.299	**0.469**	0.365	0.286	0.169	0.188	**<u>0.096</u>**	0.170	0.104
27268	0.222	0.263	0.272	0.215	0.205	0.228	**0.320**	0.311	0.247	0.152	0.219	0.115	0.132	**<u>0.098</u>**

From Table 4 it is evident that the maximum AI mean value on September 8th was located north of the study region, in the Cordillera, the coasts of the Gulf of California, and the Pacific. Superimposing the maximum/minimum mean values in Table 4 onto Fig. 1, a longitude and latitude gradient is noted, especially in the north basins located in the central mountain range and on the Pacific and the Gulf of California coasts. It seems that the trajectory of tropical storm Julio passed over the center of the peninsula and headed northward, and that it did not affect the entire study area in the same manner.

The maximum mean values observed in December and January seem to coincide with the winter rainy season. In the south and central basins an evident effect of the Pacific coast is noted. On the other hand, the rugged topography is a factor in the central basins. The results recorded for basins 14808 and 14895 deserve special emphasis; on September's date they registered their maximum mean value, while in early October their minimum.

These results may provide evidence for the relation of holding water and soil texture. On basin 14895 a balanced soil texture (clay 24.0%; sand 48.6%; loam 26.1%) is observed while a sandier texture (70.6%) for basin 14808. This suggests that the geomorphologic characteristics and soil permeability for basin 14895 enhanced the soil water holding rate in lower ground horizons but not in the upper layers where the evaporation rate might increase. The permeability of the substrate, favored by a finer soil texture, enabled this phenomenon. Furthermore, basin 14808 with a sandier soil texture obviously seems to favor vertical rainwater runoff (infiltration). Another assumed, but not visible, factor for explaining this phenomenon is the role of biological soil crusts, as Burgheimer, et al. (2006) mention; there is a rapid change in the physiological activity of the crusts after wetting, something also detected in NDVI values. The greatest change in NDVI values occur after the crust becomes wet; as the crust dries out, NDVI values decline. At regional scale, our results seem to evident the horizontal and vertical motion of rainwater and its close relation with soil texture and merit more attention for future research questions, which involve field data collection, but it is beyond the scope of this manuscript.

Geological Fractures

Statistical analysis results for fractures and for the areas between their parallel buffer lines were not significant ($p > 0.05$). Our results contradict those reported by Sonderegger (1970) who indicated that fracture traces are helpful for interpreting the presence and movement of groundwater; this is also mentioned by Aich and Gross (2008) who state that strong correlations in orientation and proximity demonstrate that bedrock fractures may strongly influence the distribution of vegetation in arid environments, especially where bedrock constitutes the greatest proportion of land cover and soils are thin. Hanson (1972) mentions that fracture traces are the surface reflection of a concentrated zone of subsurface fractures and so they should delineate zones of increased porosity and permeability. Since our results are not consistent with these reports, we need to mention that the fracture lines were digitized based on a photo interpretation of a large scale map (having a scale of 1:250,000 – that is, 1 map unit equals to 250,000 terrain units); consequently, the fracture-size features may not correctly represent real terrain, indicating that analysis results may be misinterpreted due to the difference in scale between line features and the spatial grid resolution of AI. This doesn't mean, of course, that the process for tracing fractures and buffer lines embodies inherent problems for matching themes with significant differences in spatial resolution. We consider this issue as beyond the present study and we favor further research in this area, which would include both a field campaign to validate fracture routes along with measuring devices for determining vertical water movement.

DISCUSSION

The use of remotely sensed images for studying arid regions, combined with soil permeability properties pertaining to soil water retention, has provided knowledge about the spatial variation of rainfall in semi-arid ecosystems. The use of 14 Landsat 5 TM images in one hydrological cycle has allowed us to study the vegetation response in 14 basins located on the Baja California Peninsula during a relatively atypical cycle, characterized by the influence of tropical storm Julio in mid-summer. To the best of our knowledge, this is the first attempt on this scale of observation to use such an extensive seasonal time-series to trace ecosystem dynamism and the condition of vegetation in this semi-arid region. This procedure allowed us to explore, using the aridity index, the seasonal condition of vegetation throughout the hydrologic cycle, which included: a) a dry season, b) a rainy winter season, and c) an early and mid-spring season.

Our results demonstrate the usefulness of AI to explore the role of geological strata on surface soil moisture and water retention when present, affirming the fact that a sandier soil texture favors greater vertical infiltration than a soil with balanced texture which, in turn, promotes surface runoff, evaporation, and water retention in deeper horizons. Sandy soils have larger particles and pores; this characteristic means that although these soils can hold large amounts of water, they do not retain it very long, since it leaks through the pores. A balanced texture of clay, sand, and loam, is on the opposite end of the spectrum: it has smaller particles and pores, which promote low porosity and high water retention. Aware that our study did not include soil sampling, we assumed, based on our results, that reflectance data (the data origin for the AI) broadly included all soil and vegetation factors affecting its value, such as biotic composition, soil mineral composition, soil moisture, organic matter content, and surface soil texture. But others factors remain undetectable along with their contribution to reflectance value. Consequently, pertaining AI, biological soil crusts clearly contrast with perennial plants because dry crust reflectance is generally lower than that of bare soil. Karnieli et al. (1999) found that the chlorophyll content of crusts was much higher after 7 days of incubation and showed high correlation with the NDVI values (r^2= 0.89). Furthermore, we want to mention that the AI can be useful as an indicator for many physiological and ecological parameters in semiarid ecosystems, but this topic is beyond the scope of the present study.

On basin scale, our results show that the AI in some way reveals the spatial variation of vegetation and water availability on landscape. In theory, the variability in AI observed among basins may be related to natural disturbances and also those triggered by the atypical amounts of rain occurring during the dry season. We assumed an equal spatial distribution of rain on the entire study area but our results demonstrate that the aridity condition of the north and central basins was strongly influenced by an excess of water in the swath of tropical storm Julio. Due to the absence of ground devices for registering meteorologically variable data, the exact swath of tropical storm

Julio is unclear, as is the extent and intensity of precipitated water. The spatial rainfall events on the entire study region certainly affect soil-water storage reserve and plant biomass production, but we were unable to probe the dimensionality.

Although the positive relationship between rainfall and primary productivity in arid systems is well documented in terrain experiments and through spectral indices, the consequences of this relationship on landscape composition are not well defined. The reason for this fact is that the bigger the ecosystem is, the understanding of the relationships among precipitation, primary plant productivity, heterogeneity in resource availability throughout space and time, runoff, soil moisture content, and infiltration processes become more complex.

In general, an increase in the AI value may occur as a consequence of an increase in photosynthetic activity and plant green-up; likewise an augmentation in the number of individuals in plant communities may be favored by lower water stress.

This work spans a single hydrologic cycle. Nevertheless, our results definitely suggest that long-term studies may provide opportunities for comprehending the mechanisms underlying any apparent inconsistency. Future studies should consider incorporating a larger time-series of satellite data and include landscape exclusion areas well characterized by plant biotic communities, geomorphology, roughness, land use, and climate. These areas may be useful for validating satellite derived products in such a way that they reduce the distance between real world as seen in the ecosystem and the remotely sensed world as seen by the satellite. In addition, they would provide data spanning the range of variation that individual sites experience through ecological time scales. According to Cao et al. (2004) an accurate monitoring system will help 1) to indicate the status and change in ecosystem conditions during disturbance, recovery and deterioration; 2) to predict carbon storage and the bio-geochemical dynamics of terrestrial ecosystems (Polly et al. 2005); and 3) to predict the effect of climate change on ecosystems (Coughenour and Chen 1997).

CONCLUSIONS

Our study, evaluating AI time-series over the semiarid region of the Baja California Peninsula and the different physiographic units among basins can explain the state of vegetation aridity throughout a single hydrologic cycle. It reinforces the use of satellite-derived indices for regional characterization of the ecosystem's dynamism in conjunction with geological data and land use. Closer in time with an abnormal amount of water from a tropical storm, one date of the serial AI data enhances the importance of antecedent rainfall events for comprehending the response of ecosystems to rainfall events. In a general way, a rain pulse event was observed. Our findings also seem

to emphasize the need of further research for extending the study to include more time-series data and other satellite platforms, as TRMM (Tropical Rainfall Measurement Mission), and to enrich the dataset with daily rainfall data.

ACKNOWLEDGEMENTS

REFERENCES

Abbott, M.B., Refsgaard, J.C. (1996). Distributed Hydrological Modelling. Kluwer Academic Publishers, Dordrecht, Netherlands.

Balba, A. M. (1995) Management of problem soils in arid ecosystems. CRC Press, 250 p

Aich, S. & Gross, M.R. (2008). Geospatial analysis of the association between bedrock fractures and vegetation in an arid environment. International Journal of remote sensing, 29(23), 6937-6955

Anderson, W. B., Wait, D. A. & Stapp, P. (2008). Resources from another place and time: responses to pulses in a spatially subsidized system. Ecology 89, 660–670.

Arora, V. K. (2002). The use of the aridity index to assess climate change effect on annual runoff. Journal of Hydrology 265(1–4), 164–177.

Bedford, D.R., Miller, D.M., Schmidt, K.M., & Phelps, G.A. (2009). Landscape-scale relationships between superficial geology, soil texture, topography and creosote bush size and density in the eastern Mojave Desert of California, in: Webb, R.H., Fenstermaker, L., Heaton, J.S., Hughson, D.L., McDonald, E.V., Miller, D.M. (Eds.), The Mojave Desert: Ecosystem processes and sustainability. University of Nevada Press, Reno, pp. 252-277.

Burgan, R.E., & Hartford, R.A. (1993). Monitoring Vegetation Greenness with Satellite Data, Gen. Tech. Rep. DNT-297, U.S. Department of Agriculture, Forest Service, Intermountain Research Station, Ogden, Utah, 13 p.

Burgheimer, J., Wilske, B., Maseyk, K., Karnieli, A., Zaady, E., Yakir, D., & Kesselmeier, J. (2006). Relationships between Normalized Difference Vegetation Index (NDVI) and carbon fluxes of biologic soil crusts assessed by ground measurements. Journal of arid environments 64, 651-669

Cao, M., Stephen, D.P., Small, J., & Goetz, S.J. (2004). Remotely sensed interannual variations and trends in terrestrial net primary productivity 1981–2000. Ecosystems 7, 233–242.

Chesson, P., Gebauer R.L., Schwinning, S., Huntly, N., Wiegand, K., Ernest, M.S., Sher, A., Novoplansky, A., & Weltzin, J.F. (2004). Resource pulses, species interactions, and diversity maintenance in arid and semi-arid environments. Oecologia 141, 236–253.

Cotton and Western Minning, Inc. (2008). Baja California geological summary. Magnetite seams of the Guadalupe iron mine. http://gaskinsco.com/crwn-baja.pdf [Accessed: 11 September 2013]

Coughenour, M.B. & Chen, D. (1997). Assessment of grassland ecosystem responses to atmospheric change using linked plant-soil process model. Ecological Applications 7, 802–827.

Daesslé, L.W., Ruiz-Montoya, H.J., Tobschall, R., Chandrajith, R., Camacho-Ibar, V.F., Mendoza-Espinoza, L.G., Quintanilla-Montoya, A.L. & Lugo-Ibarra, K.C. (2008). Fluoride, nitrate and water hardness in groundwater supplied to the rural communities of Ensenada County, Baja California, Mexico. Environ Geol, doi:10.1007/s00254-008-1512-9

Dettinger, M. (2004). Fifty-two years of "pineapple express" storms across the west coast of North America. U.S. Geological Survey, Scripps Institution of Oceanography for the California Energy Commission, Public Interest Energy Program, pp. 1-20.

Douglas, M.W., Maddox, R.A., Howard, K., & Reyes, S. (1993). The Mexican monsoon. Journal of Climate, 6, 1665-1677.

Franco-Vizcaino, E., Graham, R.C., & Alexander, E.B. (1993). Plant species diversity and chemical properties of soils in the central desert of Baja California, Mexico. Soil Science, 155, 406-416.

Gao, B.C. (1996). NDWI-A normalized difference water index for remote sensing of vegetation liquid water from space. Remote Sensing of Environment, 58, 257-266

Gastil, R.G., Phillips, R.P., & Allison, E.C. (1975). Reconnaissance geology of the state of Baja California. Geological Society of America Memoir 140.

Gourley, J.J., & Vieux, B.E. (2006). A method for identifying sources of model uncertainty in rainfall-runoff simulations. Journal of Hydrology, 327 (1-2), 68-80.

Graham, R.C. & Franco-Vizcaino, E. (1992). Soils on igneous and metavolcanic rocks in the Sonoran Desert of Baja California. Geoderma, 54, 1-21.

Hanson, B.C. (1972). Fracture analysis employing remote sensing techniques for groundwater movement with environmental applications: preliminary report. Arkansas academy of science proceedings, 26, 41-42

Hardisky, M. A., Klemas, V., & Smart, R. M. (1983). The influences of soil salinity, growth form, and leaf moisture on the spectral reflectance of Spartina alterniflora canopies. Photogrammetric Engineering and Remote Sensing, 49, 77−83.

He, X., Vejen, F., Stisen, S., Sonnenborg, T.O., & Jensen, K.H. (2011). An operational weather radar-based quantitative precipitation estimation and its application in catchment water resources modeling. Vadose Zone J., 10 (1), 8–24.

Jackson, T.J. Chen, D., Cosh, M., Li, F., Anderson, M., Walthall, C., Diraswammy, P. & Hunt, R.E. (2004). Vegetation water content mapping using Landsat data derived normalized difference water index for corn and soybeans, Remote sensing of Environment, 92, 475-482.

Jenny, H. (1941). Factors of soil formation: a system of quantitative pedology. McGraw-Hill Book Co. Inc., New York.

Karnielli, A., Kidron, G.J., Glaesser, C., & Ben-dor, E. (1999). Spectral characteristics of cyanobacteria soil crust in semiarid environments. Remote sensing of environment, 69 (1), 67-75.

Kogan, E.N. (1990). Remote sensing of weather impacts on vegetation. International Journal of Remote Sensing, 11, 1405-1419.

Kogan, E.N. (1995). Droughts of the late 1980's in the United States as derived from NOAA polar-orbiting satellite data. Bulletin of the American Meteorological Society, 76, 655-668.

Kurtzman, D., Navon, S., & Morin, E. (2009). Improving interpolation of daily precipitation for hydrologic modelling: spatial patterns of preferred interpolators. Hydrological Processes, 23, 3281–3291.

Liang, S., Rui, S., Xiaowen, L., Huailiang, C. & Xuefen, Z. (2011). Estimating Evapotranspiration Using Improved Fractional Vegetation Cover and Land Surface Temperature Space. J. Resour. Ecol., 2(3), 225-231.

Matin, S. & Goswami, S.B. (2012). Dryland characterization through geospatial techniques: A review. International Journal of Remote Sensing and Geoscience, 1 (1), 34-41.

Maxwell, R.M. (2010). Infiltration in arid environments: spatial patterns between subsurface heterogeneity and water-energy balances. Vadose zone J., doi:10.2136/vzj2010.0014

Newman, B.D., Wilcox, B.P., Archer, S.R., Breshears, D.D., Dahm, C.N., Duff, C.J., McDowell, N.G., Phillips, F.M., Scanlon, B.R. & Vivoni, E.R. (2006). Ecohydrology of water-limited environments: A scientific vision. Water Resour. Res., doi:10.1029/2005wr004141.

NIST/SEMATECH e-handbook of statistical methods. http://www.itl.nist.gov/div898/handbook/ [Accessed: 02 May 2015].

Noy-Meir, I. (1973). Desert ecosystems: environment and producers. Annual Review of Ecology and Systematics 4, 25–51.

Peters, A.J., WalterShea, E.A., Ji, L., Viña, A. Hayes, M., & Svoboda, M.D. (2002). Drought monitoring with NDVI-based standardized vegetation index. Photogrammetric Engineering & Remote Sensing, 268(1), 71-75.

Polly, H.W., Jonson, H.B., & Derner, J.D. (2005). Increasing CO_2 from subambient to superambient concentrations alters species composition and increases above-ground biomass in C3/C4 grassland. New Phytologist 160, 319–327.

Reyes, S., & Mejía-Trejo, A. (1991). Tropical perturbations in the eastern Pacific and the precipitation field over north-western Mexico in relation to the ENSO phenomenon. International Journal of Climatology 11, 515-528.

Rodríguez-Moreno, V.M. & Bullock, S.H. (2013). Comparison of vegetation indexes in the Sonoran desert incorporating soil and moisture indicators and application to estimates of LAI. Revista Mexicana de ciencias agrícolas, 4(4), 611-623.

Rodrìguez-Moreno & Bullock, S. H. (2015). Vegetation response to rainfall pulses in a semiarid region of Baja California. International Journal of Climatology, 34, 3967-3976.

Royston, J.P. (1995). A remark on algorithm AS181: The W-test for normality. Applied Statistics, 44, 547-551.

Sawunyama, T. & Hughes, D.A. (2008). Application of satellite-derived rainfall estimates to extend water resource simulation modelling in South Africa. Water SA, 34, 1-9.

Scanlon, B.R., Healy, R.W. & Cook, P.G. (2002). Choosing appropriate techniques for quantifying groundwater recharge. Hydrogeol, J., 10, 18-39.

Scanlon, B.R., Keese, K., Reedy, R.C., Šimůnek, J., & Andraski, B.J. (2003). Variations in flow and transport in thick desert vadose zones in response to paleoclimatic forcing (0–90 kyr): Field measurements, modeling, and uncertainities. Water Resour. Res, doi:10.1029/2002WR001604.

Scanlon, B.R., Levitt, D.G., Reedy, R.C., Keese, K.E. & Sully, M.J. (2005). Ecological controls on water-cycle response to climate variability in deserts. Proc. Natl. Acad. Sci., 102, 6033–6038.

Schwinning, S. & Sala, E. (2004). Hierarchy of responses to resource pulses in arid and semi-arid ecosystems. Oecologia, 141, 211–220.

Sonderegger, J.L. (1970). Hydrology of limestone terrains. Alabama Geol. Sur., Div. Water resources Bull, 94, 1-27.

Taesombat, W. & Sriwongsitanon, N. (2009). Areal rainfall estimation using spatial interpolation techniques. Science Asia, 35, 268–275.

Tuğrul, A. (2004). The effect of weathering on pore geometry and compressive strength of selected rock types from Turkey. Engineering Geology, 75, 215-227.

Tweed, S.O., Leblanc, M., Webb, J.A., & Lubczynski, M.W. (2006). Remote sensing and GIS for mapping groundwater recharge and discharge areas in salinity prone catchments, southeastern Australia. Hydrogeology Journal, 15, 75-96.

Walvoord, M.A., Plummer, M.A., Phillips, F.M. & Wolfsberg, A.V. (2002). Deep arid system hydrodynamics: 1. Equilibrium states and response times in thick desert vadose zones. Water Resour. Res., doi:10.1029/2001WR000824.

Wang, H., Kgotlhang, L. & Kinzelbach, W. (2008). Using remote sensing data to model groundwater recharge potential in Kanye region, Botswana. The International Archives of the Photogrammetry, Remote Sensing and Spatial Information Sciences 37, Part B8. Beijing 2008.

West, N. E. (1990). Structure and function of microphytic soil ISSS International Symposium (Working Groups RS and crust in wildland ecosystems of arid to semi-arid regions. DM) on Monitoring Soils in the Environment with Remote Adv. Ecol. Res. 20, 179–223.